RESEARCH ARTICLE

Ex vivo confocal laser scanning microscopy: A diagnostic technique for easy real-time evaluation of benign and malignant skin tumours

Gabriela Vladimirova[1] | Cristel Ruini[1,2]* | Florian Kapp[1] |
Benjamin Kendziora[1] | Ecem Z. Ergün[1,3] | Işın S. Bağcı[4] |
Sebastian Krammer[1] | Jawaher Jastaneyah[1] | Elke C. Sattler[1] |
Michael J. Flaig[1] | Lars E. French[1,5] | Daniela Hartmann[1]

[1]Department of Dermatology and Allergy, University Hospital, LMU Munich, Munich, Germany

[2]PhD School in Clinical and Experimental Medicine, University of Modena and Reggio Emilia, Modena, Italy

[3]Department of Dermatology and Venereology, Istanbul Training and Research Hospital, Org. Abdurrahman Nafiz Gürman Cad. Etyemez, Istanbul, Turkey

[4]Department of Dermatology, Stanford University School of Medicine, Redwood City, California, USA

[5]Dr. Phillip Frost Department of Dermatology & Cutaneous Surgery, University of Miami, Miller School of Medicine, Miami, Florida, USA
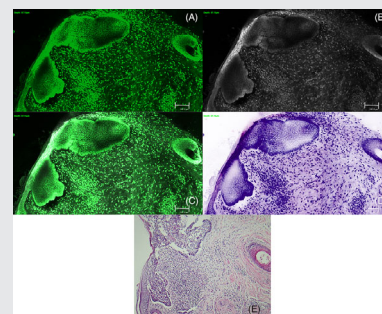
*Correspondence
Cristel Ruini, Department of Dermatology and Allergy, University Hospital, LMU Munich, Frauenlobstrasse 9-11, 80337 Munich, Germany.
Email: cristel.ruini@med.uni-muenchen.de

Abstract

Ex vivo confocal laser scanning microscopy (ex vivo CLSM) is a novel diagnostic tool for a quick bedside evaluation of freshly excised tissue, comparable to histology. We aimed to assess the sensitivity and specificity of ex vivo CLSM in detecting malignant features, to validate its reliability in identifying various skin tumours based on a combination of confocal features and to evaluate the digital staining mode (DS). One-hundred twenty freshly excised skin samples from 91 patients were evaluated. Each lesion was screened for the presence of 23 predefined confocal criteria with ex vivo CLSM, followed by a histopathological examination. The diagnostic agreement between ex vivo CLSM and histology was 89.2%. The diagnostic accuracy of ex vivo CLSM in detecting malignancy reached a sensitivity of 98% and a specificity of 76%. Ex vivo CLSM enabled a rapid identification of the most common skin tumours, the tumour dignity and cytological features. The DS demonstrated a close resemblance to conventional histopathology.

1 | INTRODUCTION

The incidence of skin tumours shows an increasing rate worldwide; hence, there is a high demand for diagnostic tools for fast, easy and reliable tumour examination and tissue assessment [1]. The gold standard diagnostic method for skin tumours is the histopathological examination of excised tissue [2]. Additionally, other tools could extend the diagnostic portfolio for skin lesions. Namely, the ex vivo confocal laser scanning microscopy (CLSM) that can be applied directly on freshly excised and frozen tissues in order to produce immediate microscopic images in an intraoperative setting. This diagnostic method, commonly named bedside histology, provides high-resolution vertical images of the excised specimen without a depth limitation, known from the horizontal in vivo CLSM images, allowing for the examination of all tissue layers, comparable to conventional histopathology [3].

In addition, the current new generation of the ex vivo device (Vivascope 2500M-G4, Lucid Inc., Rochester, New York) offers a new digital staining tool, so-called digital haematoxylin-eosin-like (H&E) mode. A special software combines the green fluorescence mosaics and the grayscale reflectance mosaics into an overlay image, which is further elaborated and generates purple and pink images similar to conventional H&E staining. This allows a direct comparison to the gold standard histological examination.

Ex vivo CLSM has already been used in several fields of dermatology, including benign and malignant skin tumours [4–7], as well as inflammatory and infectious diseases [8–10], and healthy skin [11]. A successful use of fluorescent-labelled antibodies (Ber-EP4, S100 and Melan A) in combination with the ex vivo CLSM on melanocytic and non-melanocytic skin tumours has been described [12]. It has also been used to detect autoimmune complexes in cutaneous vasculitis [13], bullous pemphigoid [14], pemphigus vulgaris [15, 16], cutaneous lupus erythematosus [17] and lichen planus [18] with comparable performance to conventional direct immunofluorescence microscopy.

In dermato-oncology, ex vivo CLSM has been primarily used for intraoperative determination of tumour margins during Mohs surgery [19–21]. Ex vivo CLSM diagnostic criteria and disease patterns have been described for various skin tumours, such as basal cell carcinoma (BCC) and squamous cell carcinoma (SCC), to facilitate the diagnosis and tumour differentiation [22,

23]. In addition, ex vivo CLSM has been used to measure Breslow thickness in melanoma allowing the treating physician to get valuable information on prognosis and treatment choices directly intraoperatively [24].

Until now only few studies have assessed the diagnostic accuracy of the latest ex vivo CLSM device including the novel digital H&E staining mode [25, 26]. The objective of this study was to describe ex vivo confocal characteristics of the most common benign and malignant skin tumours, using the newest ex vivo CLSM generation, in comparison with conventional histopathology.

2 | PATIENTS AND METHODS

2.1 | Study site, study team and tissue samples

From January 2019 to June 2019, 120 samples from 91 patients with various benign and malignant skin tumours, including BCC, SCC, basosquamous carcinoma (BSC), actinic keratosis (AK), Bowen's disease (BD), melanoma (MM), melanoma metastasis, Merkel cell carcinoma (MCC), atypical fibroxanthoma (AFX), verruca vulgaris (VV), fibroma, dermal nevus (DN), neurofibroma (NF), molluscum contagiosum (MC) and condyloma acuminatum (CA), were collected for examination with ex vivo CLSM. The tissue probes were collected at the Dermatological Surgery Unit of the Department of Dermatology and Allergy, University Hospital, LMU Munich, Germany, after gathering written informed consent from each participant preoperatively. The study was carried out according to the Declaration of Helsinki and was approved by the Ethics committee of the Ludwig Maximilian University, Munich, Germany (Protocol Nr. 19-150). The ex vivo CLSM examination and the comparison of confocal and histopathological images were independently performed by two specially trained dermatologists. The investigators were blinded to the histological diagnosis.

2.2 | Ex vivo CLSM device

The commercially available ex vivo CLSM (VivaScope 2500M-G4; Lucid Inc., Rochester, New York) uses two lasers, operating at wavelengths of 488 nm (blue) and

785 nm (infrared) and performs simultaneous tissue examination in the reflectance mode (RM), fluorescence mode (FM), overlay mode (OM) and digital staining mode (DS). The device has a horizontal resolution of less than 1.25 μm, vertical resolution of less than 5 μm and a maximum imaging depth of 200 μm depending on the tissue type. Magnification reaches up to 550-fold with an image resolution of 1024 × 1024 pixel. The acquisition time of the device varies between 1 and 4 minutes, depending on the size of the scanned tissue sample.

2.3 | Ex vivo CLSM examination

The freshly excised tissue samples were processed immediately postoperatively for examination. All specimens were examined unaltered to avoid any tissue damage. During the ex vivo CLSM examination, all studied samples were stained with Acridine Orange (0.6 mM; Sigma-Aldrich, Merck KGaA) for 30 seconds. To remove the excess stain, they were then rinsed with phosphate buffered saline (PBS, Sigma-Aldrich, Merck KGaA) for 30 seconds. Afterwards, the tissue probes were treated with 10% citric acid for 30 seconds and were rinsed once again with PBS (Sigma-Aldrich, Merck KGaA). Finally, the tissue flattening technique using a system of magnets and sponges, described by Pérez-Anker et al., was applied for image acquisition [27]. The tissue samples were scanned vertically to provide exact correlation to the subsequent conventional histopathological slides.

2.4 | Conventional histopathological examination

Since ex vivo CLSM causes no damage to the excised tissue, all examined probes were subsequently fixed in formalin, embedded in paraffin and stained for conventional histopathology. The slides were then independently examined in the Dermatopathology department. Selected histological features were correlated with CLSM features and were statistically analysed.

2.5 | Evaluation of microscopic features

The criteria analysed in our study were determined according to past studies and were based on previously described CLSM criteria [6, 11, 22–24, 28], our experience and common histopathological diagnostic criteria. The following criteria were evaluated in each specimen: hyperkeratosis, parakeratosis, erosion/ulceration, acanthosis, papillomatosis, architectural disarray of the epidermis and/or dermis, atypical keratinocytes in the epidermis, atypical melanocytes in the epidermis, actinic elastosis, loose connective tissue with dilated capillaries, basal hyperpigmentation, koilocytes, presence of tumour mass in the dermis or subcutis, clefting, peripheral palisading, nuclear pleomorphism, stromal reaction, atypical keratinocytes in the dermis, keratin pearls, atypical melanocytes in the dermis, loss of maturation of dermal melanocytes, mitoses in the tumour cells in the dermis and presence of peritumoural inflammatory infiltrate. All images were examined in RM, FM, OM and DS.

2.6 | Statistical analysis

We calculated the overall diagnostic agreement between ex vivo CLSM and conventional histopathology. Sensitivity, specificity, positive predictive value (PPV), negative predictive value (NPV), area under the receiver operating characteristic curve (AUC, ROC) and Cohen's kappa coefficient were calculated for ex vivo CLSM in the subgroup of malignant tumours and in all diagnoses, with a case number of n ≥ 10 and the 23 histological characteristics mentioned above.

Cohen's kappa coefficient was interpreted as follows: no agreement (kappa score less than 0), slight agreement (kappa score between 0.00 and 0.20), fair agreement (kappa score between 0.21 and 0.40), moderate agreement (kappa score between 0.41 and 0.60), substantial agreement (kappa score between 0.61 and 0.80) and almost perfect agreement (kappa score between 0.81 and 1.00). R, version 3.6.0, 2019, R Foundation for Statistical Computing, was used for all statistical calculations. The following R packages were applied: DescTools [29], pROC [30] and ggplot2 [31].

3 | RESULTS

One-hundred twenty tissue probes from 91 patients, 33 women (36%) and 58 men (64%), were examined with ex vivo CLSM and conventional histology in this study. The mean age of the participants was 74.3 years (95% CI: 70.9, 77.7). The average number of lesions per patient was 1.2 (95%CI: 1.0, 1.4). Forty-six samples of BCC, 27 of SCC, 3 of BD, 10 of AK, 2 of MM, 1 of melanoma metastasis, 1 of MCC, 1 of AFX, 1 of NF, 7 of fibroma, 1 of DN, 2 of VV, 2 of MC, 1 of CA, 1 of BSC, and 1 of SCC + AK were histologically proven. Thirteen skin specimens were tumour-free. The nose was the most common site for BCC, followed by the scalp and the ears. Most of the invasive SCC appeared on the scalp, followed by the cheeks and the nose, and most of the in situ SCC were found on the forehead, followed by the scalp and nose.

TABLE 1   Diagnostic accuracy of ex vivo confocal laser scanning microscopy (ex vivo CLSM) in identifying 23 predefined histopathological characteristics

	Present in x cases	Sensitivity	CI Lower	CI Upper	Specificity	CI Lower	CI Upper	PPV	CI Lower	CI Upper	NPV	CI Lower	CI Upper	AUC	CI Lower	CI Upper	κ	CI Lower	CI Upper
Hyperkeratosis	72	0.93	0.85	0.98	1.00	0.89	1.00	1.00	0.95	1.00	0.86	0.71	0.95	0.97	0.94	0.99	0.89	0.80	0.98
Parakeratosis	34	0.97	0.85	1.00	0.96	0.88	0.99	0.92	0.78	0.98	0.99	0.92	1.00	0.96	0.93	1.00	0.91	0.83	1.00
Erosion/Ulceration	29	0.93	0.77	0.99	0.96	0.89	0.99	0.90	0.73	0.98	0.97	0.91	1.00	0.95	0.89	1.00	0.88	0.78	0.98
Acanthosis	31	0.90	0.74	0.98	0.96	0.88	0.99	0.90	0.74	0.98	0.96	0.88	0.99	0.93	0.87	0.99	0.86	0.75	0.97
Papillomatosis	18	0.89	0.65	0.99	0.98	0.92	1.00	0.89	0.65	0.98	0.98	0.92	1.00	0.93	0.85	1.00	0.87	0.74	0.99
Epidermal and/or dermal disarray	99	1.00	0.96	1.00	0.70	0.46	0.88	0.94	0.88	0.98	1.00	0.77	1.00	0.85	0.75	0.95	0.80	0.64	0.95
Atypical keratinocytes in the epidermis	45	0.96	0.85	0.99	0.93	0.83	0.98	0.90	0.77	0.97	0.97	0.89	1.00	0.94	0.90	0.98	0.87	0.78	0.96
Atypical melanocytes in the epidermis	2	1.00	0.16	1.00	1.00	0.97	1.00	1.00	0.16	1.00	1.00	0.97	1.00	1.00	1.00	1.00	1.00	1.00	1.00
Actinic elastosis	55	0.80	0.67	0.90	0.92	0.83	0.97	0.90	0.78	0.97	0.85	0.74	0.92	0.86	0.80	0.92	0.73	0.61	0.85
Loose connective tissue	3	1.00	0.29	1.00	1.00	0.97	1.00	1.00	0.29	1.00	1.00	0.97	1.00	1.00	1.00	1.00	1.00	1.00	1.00
Basal hyperpigmentation	2	0.50	0.01	0.99	1.00	0.97	1.00	1.00	0.03	1.00	0.99	0.95	1.00	0.75	0.26	1.00	0.66	0.04	1.00
Koilocytes	3	1.00	0.29	1.00	1.00	0.97	1.00	1.00	0.29	1.00	1.00	0.97	1.00	1.00	1.00	1.00	1.00	1.00	1.00
Tumour mass in the dermis and/or subcutis	82	0.96	0.90	0.99	0.81	0.65	0.92	0.92	0.84	0.92	0.91	0.76	0.98	0.89	0.82	0.95	0.80	0.68	0.92
Clefting	46	1.00	0.92	1.00	0.93	0.85	0.98	0.90	0.79	0.97	1.00	0.95	1.00	0.97	0.94	1.00	0.91	0.84	0.99
Palisading	46	0.98	0.88	1.00	0.95	0.87	0.99	0.92	0.80	0.98	0.99	0.92	1.00	0.96	0.93	1.00	0.91	0.84	0.99
Nuclear pleomorphism	93	0.99	0.94	1.00	0.89	0.71	0.98	0.97	0.91	0.99	0.96	0.80	1.00	0.94	0.88	1.00	0.90	0.81	1.00
Stromal reaction	52	0.81	0.67	0.90	0.96	0.88	0.99	0.93	0.82	0.99	0.87	0.77	0.93	0.88	0.82	0.94	0.78	0.66	0.89
Atypical keratinocytes in the dermis	30	0.87	0.69	0.96	0.97	0.91	0.99	0.90	0.73	0.98	0.96	0.89	0.99	0.92	0.85	0.98	0.84	0.73	0.96
Keratin pearls	20	0.75	0.51	0.91	0.99	0.95	1.00	0.94	0.70	1.00	0.95	0.89	0.98	0.87	0.77	0.97	0.80	0.65	0.95
Atypical melanocytes in the dermis	2	1.00	0.16	1.00	1.00	0.97	1.00	1.00	0.16	1.00	1.00	0.97	1.00	1.00	1.00	1.00	1.00	1.00	1.00
Loss of maturation of dermal melanocytes	1	1.00	0.03	1.00	1.00	0.97	1.00	1.00	0.03	1.00	1.00	0.97	1.00	1.00	x	x	1.00	1.00	1.00
Mitosis of dermal tumour cells	35	0.66	0.48	0.81	0.95	0.88	0.99	0.85	0.66	0.85	0.87	0.78	0.93	0.80	0.72	0.89	0.65	0.50	0.81
Inflammatory infiltrate	106	0.92	0.84	0.96	0.93	0.66	1.00	0.99	0.94	1.00	0.59	0.36	0.79	0.80	0.72	0.89	0.68	0.49	0.86

Abbreviations: AUC, area under the receiver operating curve; ex vivo CLSM, ex vivo confocal laser scanning microscopy; NPV, negative predictive value; PPV, positive predictive value.

3.1 | Overall diagnostic agreement

The overall diagnostic agreement between ex vivo CLSM and conventional histopathology was 89.2% (95% CI: 82.2, 94.1). Of the 120 histopathological diagnoses, 107 were correctly identified by ex vivo CLSM.

3.2 | Histological features

The results of accuracy of CLSM in identifying the previously mentioned 23 microscopic features are listed in Table 1. Overall, 15 features showed an almost perfect and 8 features a substantial agreement with histopathology.

3.3 | Malignancy and premalignancy

BCC, SCC, MM, melanoma metastasis, MCC, AFX, BSC, BD and AK were classified as malignant/premalignant. The apparent prevalence of malignancy and premalignancy (CLSM) amounted to 80%, while the true prevalence (conventional histopathology) was 76%. Ex vivo CLSM reached an overall sensitivity in detecting malignancy of 98% and an overall specificity of 76%, with a Cohen's kappa coefficient of 0.78 and AUC of 0.87. Eighty-nine diagnoses were true positives and 22 were true negatives. The number of incorrect diagnoses was 9, with 7 false positives and 2 false
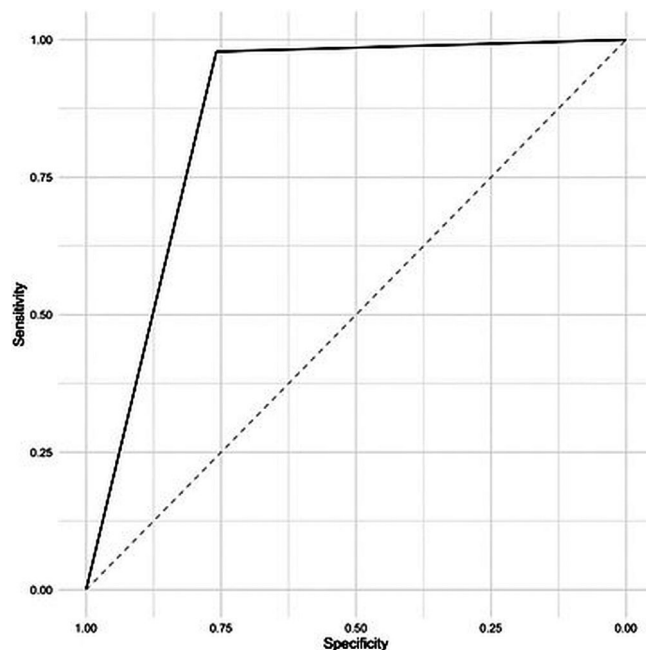

FIGURE 1 Receiver operating characteristic (ROC) curve of the diagnostic accuracy of ex vivo confocal laser scanning microscopy (ex vivo CLSM) in detecting malignancy and premalignancy

TABLE 2 Sensitivity, specificity, positive and negative predictive value, AUC and kappa score of ex vivo CLSM in detecting BCC, SCC and AK

	Sensitivity	CI Lower	CI Upper	Specificity	CI Lower	CI Upper	PPV	CI Lower	CI Upper	NPV	CI Lower	CI Upper	AUC	CI Lower	CI Upper	κ	CI Lower	CI Upper
Basal cell carcinoma	0.98	0.88	1.00	0.95	0.87	0.99	0.92	0.80	0.98	0.99	0.92	1.00	0.96	0.92	1.00	0.91	0.84	0.99
Squamous cell carcinoma	0.93	0.76	0.99	0.97	0.91	0.99	0.90	0.73	0.98	0.98	0.92	1.00	0.94	0.89	1.00	0.88	0.79	0.98
Actinic keratosis	0.82	0.48	0.98	0.97	0.92	0.99	0.75	0.43	0.95	0.98	0.93	1.00	0.90	0.77	1.00	0.76	0.56	0.96

Abbreviations: AK, actinic keratosis; AUC, area under the receiver operating curve; BCC, basal cell carcinoma; ex vivo CLSM, ex vivo confocal laser scanning microscopy; NPV, negative predictive value; PPV, positive predictive value; SCC, squamous cell carcinoma.

negatives. Figure 1 portrays the ROC curve of the diagnostic accuracy of ex vivo CLSM in detecting malignancy and premalignancy.

The diagnostic accuracy of ex vivo CLSM in identifying the following three malignant diagnoses with a case number ≥10 is illustrated in Table 2.

3.3.1 | Basal cell carcinoma

The overall agreement between ex vivo CLSM and histology in diagnosing BCC was almost perfect with a kappa score of 0.91 and an AUC of 0.96. The sensitivity of ex vivo CLSM in detecting BCC was 98% and the specificity was 95%, with a PPV of 92% and an NPV of 99%. The diagnosis of BCC was based on the presence of the typical morphologic features of this tumour type, in particular, tumour mass in the dermis and/or subcutis, clefting and palisading. In detecting these features, ex vivo CLSM demonstrated an excellent sensitivity of 96%, 100% and 98%, respectively, and specificity of 81%, 93% and 95%, respectively. Stromal reaction was another feature commonly observed in BCC imaging. Ex vivo CLSM was able to identify it with a sensitivity of 81% and a specificity of
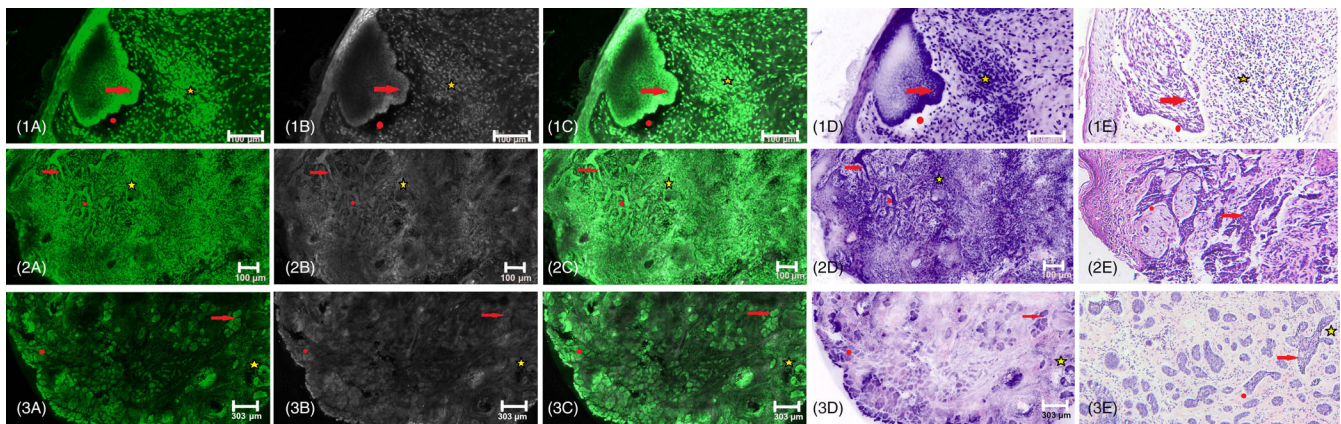

FIGURE 2 Common subtypes of basal cell carcinoma (BCC) scanned with the ex vivo confocal laser scanning microscopy (ex vivo CLSM) device (Vivascope 2500M-G4) in fluorescence mode (A), reflectance mode (B), overlay mode (C) and digital staining mode (D) and correlated to conventional histology (E): 1—superficial BCC spreading from the bottom epidermis and presenting a clear tumour mass, peripheral palisading (red arrows) of the tumour cells and clefting (red dots) between the tumour mass and the demarcated stroma (yellow stars); 2—infiltrating BCC with scattered tumour islands distributed in the stroma; and 3—micronodular BCC displaying multiple small tumour islands, peripheral palisading and clefting
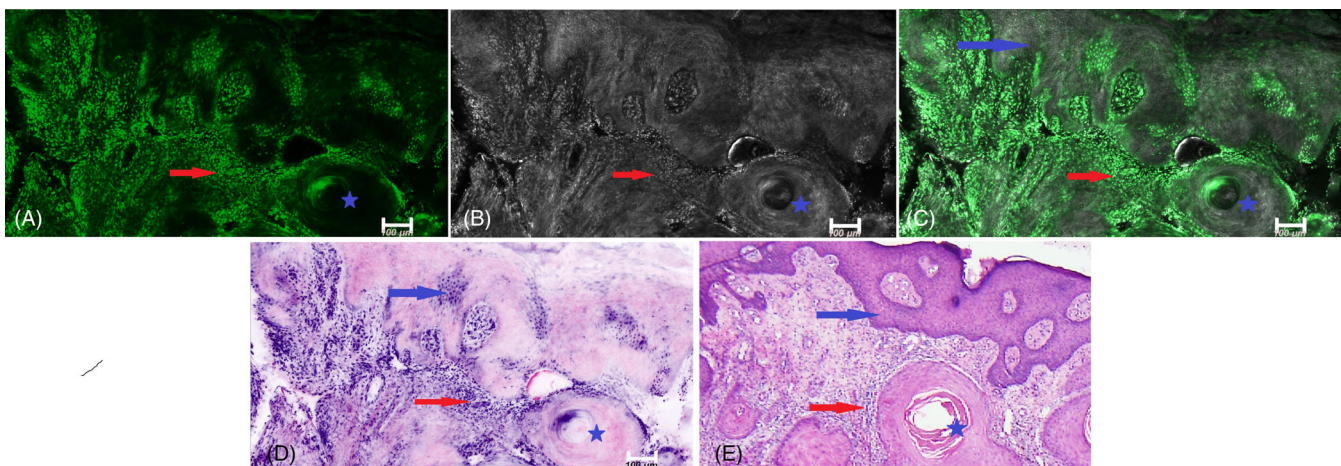

FIGURE 3 Ex vivo confocal laser scanning microscopic (ex vivo CLSM) images of a well-differentiated squamous cell carcinoma (SCC) in fluorescence mode (A), reflectance mode (B), overlay mode (C) and digital staining mode (D) compared to conventional histology (E), showing plump bright cells in the dermis, architectural disarray of the epidermis and dermis (blue arrows), inflammatory infiltrate (red arrows) and a keratin pearl (blue stars) in the bottom right corner of the images
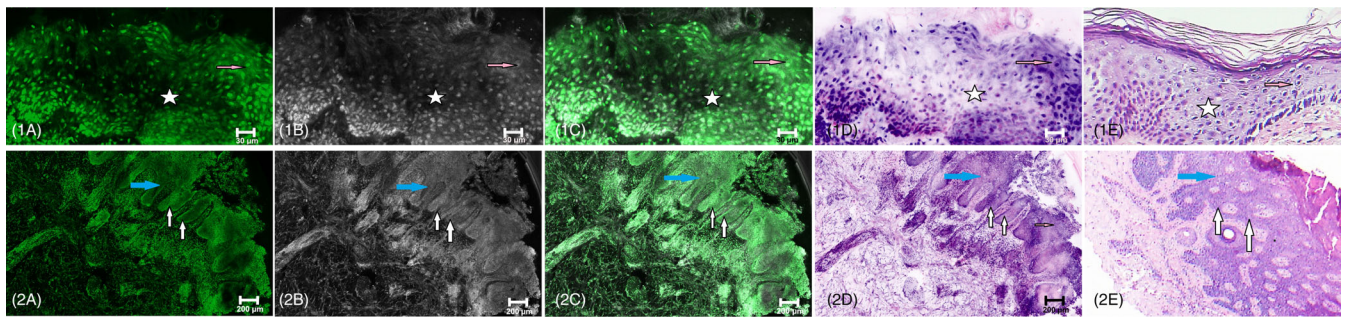
FIGURE 4 Ex vivo confocal laser scanning microscopic (ex vivo CLSM) images of premalignancy (actinic keratosis [AK] and Bowen's disease [BD]) in fluorescence mode (A), reflectance mode (B), overlay mode (C) and digital staining mode (D) compared to the images of conventional histology (E): 1—AK showing architectural disarray of the epidermis (white stars) and plump bright atypical epidermal keratinocytes (pink arrows), and 2—BD with noticeable acanthosis (blue arrows), papillomatosis (white arrows), architectural disarray of all epidermal layers and plump atypical keratinocytes limited to the epidermis (pinks arrows)
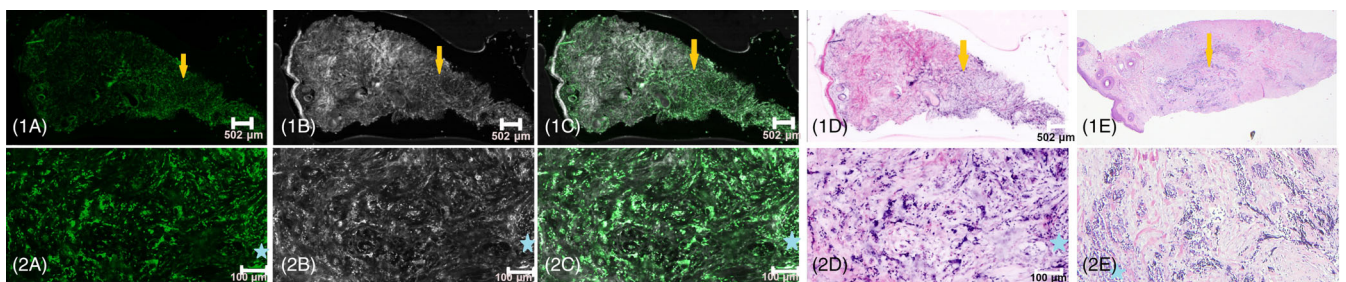

FIGURE 5 Ex vivo confocal laser scanning microscopic (ex vivo CLSM) images in different magnification grades (1—low magnification, 2—high magnification) in fluorescence mode (A), reflectance mode (B), overlay mode (C) and digital staining mode (D) of a Merkel cell carcinoma (MCC) correlated to conventional histology (E): 1—a diffuse infiltration of small tumour cells forming a wide tumour mass in the dermis (yellow arrows) as well as 2—inflammatory infiltrate (light blue stars)
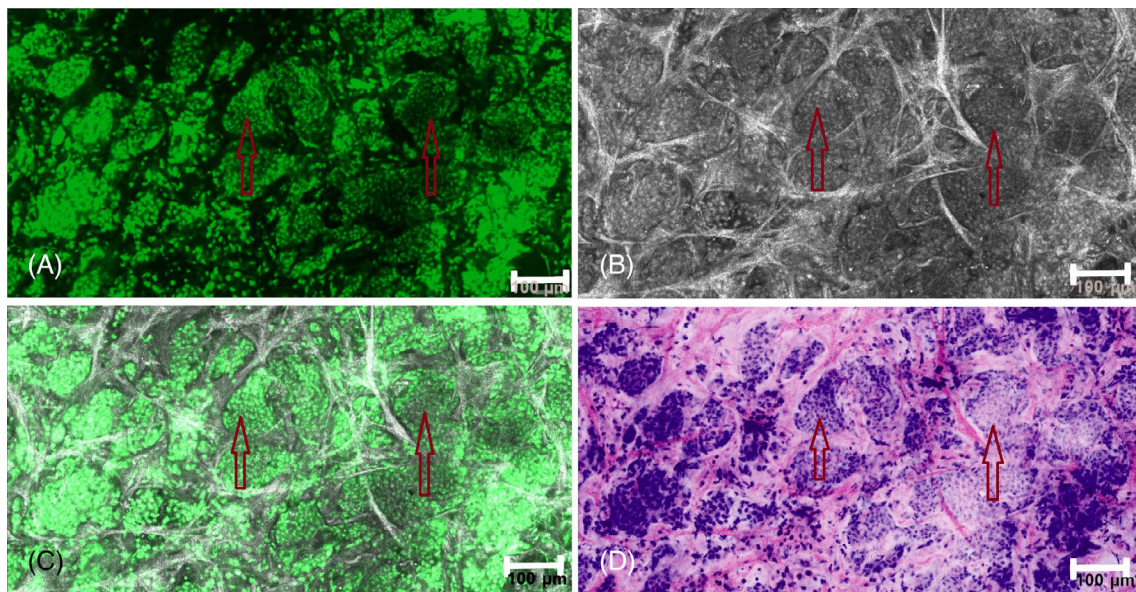

FIGURE 6 Ex vivo confocal laser scanning microscopic (ex vivo CLSM) images in fluorescence mode (A), reflectance mode (B), overlay mode (C) and digital staining mode (D) of a horizontally scanned malignant melanoma (MM) showing roundish nests of atypical melanocytes in the dermis with a high mitotic activity (dark red arrows)

96%. Examples of images of different BCC subtypes in all four modes of the ex vivo CLSM device (Vivascope 2500M-G4) are shown in Figure 2.

3.3.2 | Squamous cell carcinoma

The sensitivity of CLSM in detecting SCC was 93% (0.76, 0.99). With a specificity of 97%, a PPV of 90% and an NPV of 98%, ex vivo CLSM proved an almost perfect agreement with histology with a Cohen's kappa coefficient of 0.88 and an AUC of 0.94. Hyperkeratosis, erosion/ulceration, architectural disarray, actinic elastosis, tumour mass in the dermis and/or subcutis, nuclear pleomorphism, atypical keratinocytes in the epidermis and in the dermis, keratin pearls and inflammatory infiltrate were the features, which were most frequently observed in the CLSM images of SCC. The sensitivity and specificity values of these features are presented in Table 1. An example of the images of a well-differentiated SCC acquired with ex vivo CLSM and compared to the image of conventional histology is shown in Figure 3.

3.3.3 | Actinic keratosis

Ex vivo CLSM was able to detect AK with a sensitivity of 82% and a specificity of 97%. The PPV was 75% and the NPV was 98%. The agreement between CLSM and conventional histopathology was substantial with a kappa score of 0.76 and an AUC of 0.90. In CLSM, AK was typically presented by the combination of the following features:
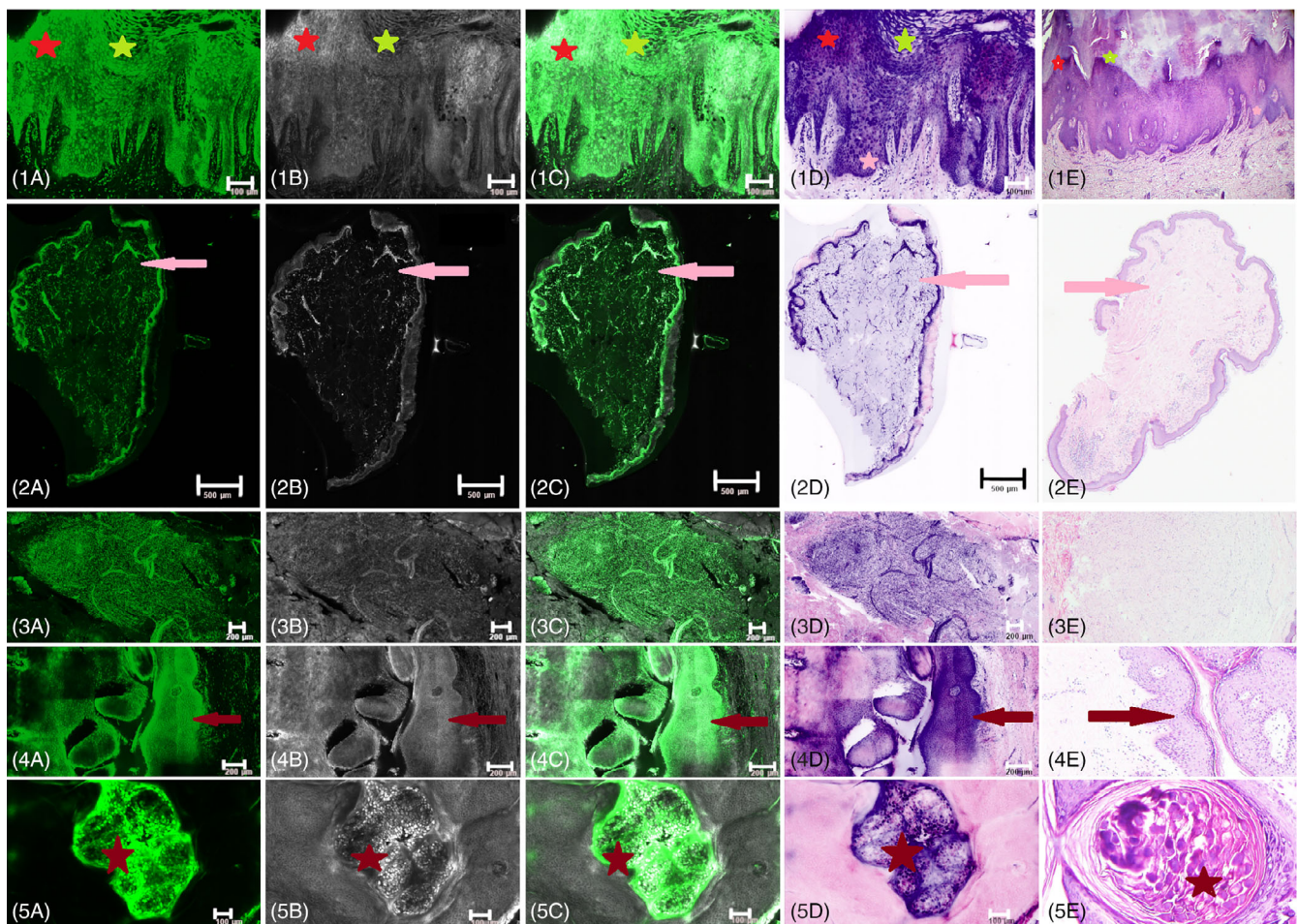

FIGURE 7   Ex vivo confocal laser scanning microscopic (ex vivo CLSM) images in fluorescence mode (A), reflectance mode (B), overlay mode (C) and digital staining mode (D) of different benign skin tumours correlated to conventional histology (E), 1—verruca vulgaris (VV) represented by an acanthotic and papillomatous epidermis with hyperkeratosis (green stars), parakeratosis (red stars) and vacuolated keratinocytes (koilocytes) (pink stars); 2—fibroma displaying a tumour mass of loose connective tissue (pink arrows); 3—neurofibroma (NF) visible as a round dermal tumour mass of monomorphous cells; 4—condyloma acuminatum (CA) showing acanthosis and papillomatosis of the epidermis (dark red arrows); and 5—molluscum contagiosum (MC) with typical large molluscum bodies (dark red stars)

architectural disarray, actinic elastosis and atypical keratinocytes in the epidermis. The results of accuracy for these features are displayed in Table 1. An example of the confocal images of an AK as well as of a BD is shown in Figure 4 directly compared to the images of conventional histology.

3.3.4 | Other malignant and premalignant skin tumours

In this study, three cases of BD were examined confocally and histopathologically and all of them were diagnosed correctly by ex vivo CLSM. The features noticed commonly in the confocal images were parakeratosis, acanthosis, papillomatosis, architectural disarray and atypical keratinocytes in the epidermis. Parakeratosis was distinguished with a sensitivity of 97% and specificity of 96%, acanthosis with a sensitivity of 90% and specificity of 96% and papillomatosis with a sensitivity of 89% and a specificity of 98%. The sensitivity and specificity for the other criteria could be found above.

Malignant tumours, such as AFX, MCC, MM and melanoma metastasis demonstrated a dermal tumour mass, a high mitotic activity and a dense inflammatory infiltrate. Ex vivo confocal images of an MCC and the corresponding histopathologic slides are presented in Figure 5. In the confocal images of all MM and melanoma metastasis, atypical melanocytes in the epidermis and dermis as well as a loss of maturation of the dermal melanocytes were present. Figure 6 shows ex vivo confocal images of an MM correlated to histology.

3.3.5 | Benign skin tumours

Most of the benign skin tumours with a case number smaller than 10 have been evaluated correctly based on morphologic features, which correspond almost perfectly with the typical histological criteria of the respective tumour type. The visual result of the DS mode was remarkably similar to the H&E-stained samples. Exemplary ex vivo confocal images of VV, fibroma, NF, condyloma and MC compared to their histopathological correlates are displayed in Figure 7.

Diagnosing VV appeared to be easy, considering the presence of hyperkeratosis, parakeratosis, acanthosis, papillomatosis, as well as the highly specific koilocytes. Ex vivo CLSM managed to detect koilocytes with a sensitivity and specificity of 100%.

Other benign tumours such as fibroma, NF, MC and DN had a defined tumour mass in the dermis/subcutis, consisting of cells from the corresponding tissue type.

The DS mode was the most useful tool for differentiating between those tissue types.

All listed diagnoses had a low or absent mitotic activity in common. Although CLSM achieved only a substantial sensitivity of 66% in detecting mitosis, the specificity was very good, in particular 95%. Loose connective tissue and basal hyperpigmentation appeared rarely and were found only in the images of fibroma. Loose connective tissue was correctly distinguished in all three positive images and basal hyperpigmentation in one of the two positive images.

The one sample of NF presented a single big dermal tumour mass of homogeneous cells, while the monomorphic tumour cells of the DM were grouped in small nests.

4 | DISCUSSION

Our study focused on the evaluation of the performance of the newest ex vivo CLSM generation in the examination of various benign and malignant skin tumours, routinely excised in the dermatological practice. All of the ex vivo CLSM images were examined simultaneously in the four modalities (FM, RM, OM and DS). According to our observation, we can clearly confirm the already stated differences in previous papers on this topic [32]. The FM, achieved by using Acridine Orange, depicts perfectly the cell nuclei and increases the contrast of cell structures, especially the cell-stroma contrast. The RM allows a detailed observation of the matrix structures, like elastic and collagen fibres. The OM combines the advantages of both modalities in one image, while the DS facilitates the examination for trained pathologists even more by creating an image of the tissue probe which is very similar to the images of conventional pathology. The integration of four different imaging modalities (FM, RM, OM and DS) has broadened the spectrum of image analysis, mainly based on two significant advantages. First, the OM now combines the visualisation of nuclear and matrix structures into one image; second, the DS reproduces the conventional H&E staining, allowing physicians trained in histopathology to recognize the common microscopic features. Since switching between the four modes is fast and easy, we evaluated all samples applying all imaging modalities as the combination of all together provided valuable information for accurate diagnostic assessment.

The sensitivity and specificity of ex vivo CLSM for diagnosing skin neoplasms was high. The overall sensitivity in detecting malignant tumours of 98% and specificity of 76%, together with an overall diagnostic agreement of 0.78 and AUC of 0.87, suggest an accurate analysis in a real-life setting. Ex vivo CLSM enabled correct recognition of most tumours and proved an overall diagnostic agreement with histology of 89.2%.

The presented study did not only focus on the overall diagnostic agreement but has also evaluated ex vivo CLSM-specific criteria corresponding to common histopathological features. We, therefore, selected a total of 23 diagnostic features visible by the ex vivo CLSM, most of whom in almost perfect agreement with histopathology, as demonstrated by Cohen kappa scores of above 0.80 and AUC of above 0.90 for the great majority of them (Table 1). The chosen diagnostic features are frequently seen in the every-day pathology practice and describe the most common characteristics of the examined diagnoses. Most of them are already well-established and recognizable using ex vivo CLSM [6, 22, 23]. Epidermal features such as erosion/ulceration, hyperkeratosis, parakeratosis, acanthosis and papillomatosis could be displayed with ex vivo CLSM. Not only architecture but also cytological features (atypical keratinocytes and melanocytes, koilocytes, immature melanocytes) were clearly recognizable. Highly specific tumour features such as palisading and clefting in BCC were also apparent. Some features such as inflammatory infiltrate and actinic elastosis were more challenging, reaching satisfactory AUCs 0.75 to 0.89 (Table 1).

Once having proven their diagnostic accuracy and reproducibility, such criteria may be implemented to various common skin tumours encountered in the daily clinical routine. We can confirm that the presented criteria for the most common malignant skin tumours (BCCs as well as in situ and invasive SCCs) allowed an almost perfect diagnostic accuracy, with AUCs > 0.90.

The results should be interpreted taking into account the limited number of DMs and MMs. The same caution applies to the other features that were rarely discovered in the samples from this study. In fact, the main limitation of this study is the small sample size of examined tumours, especially the less common ones, which cannot provide statistical significance. These findings are however based on the real-life setting of our data collection and should encourage further studies on the detection of different tumour entities with CLSM.

Even tumours with a small case number could be identified with a good accuracy based on a combination of ex vivo CLSM features. Interestingly, we found DS very useful in detecting the predefined diagnostic criteria for tumours with a small number of investigated samples. In fact, creating an image, nearly identical to an H&E section, allowed the examiners to use their histological knowledge for the interpretation of the tissue morphology. DS represents an innovation of outmost importance, making ex vivo CLSM reading easier also for dermatologists who are not trained in non-invasive diagnostic techniques. In fact, the software is able to digitally purple stain fluorescence-highlighted nuclei (mimicking haematoxylin), while reflectance-enhanced cytoplasm and matrix structures are converted to pink (mimicking eosin). The resulting image is very similar to H&E-stained tissue slides. The user can easily switch from one visualization mode to another to acquire as most details as possible during the ex vivo scanning process. Schüürmann et al. have recently described in detail the appearance of the different cytological structures of healthy skin in the DS mode [26]. A present-day publication by Reggiani et al. has even already statistically proved the superiority of DS over the other diagnostic modalities for the evaluation of BCCs by both dermatologists and pathologists by reaching impressive 94% overall correct diagnoses with a sensitivity of 83.3% and a specificity of 96.1% [33]. Although DS alone is a breakthrough in ex vivo CLSM, we strongly recommend further research on new staining methods to further increase the diagnostic accuracy of ex vivo CLSM and extend the spectrum of indications.

In conclusion, we reached a high accuracy in detecting malignant and benign skin tumours with ex vivo CLSM compared to histopathology. The device has proved to be a quick and accurate tool for the detection of malignant and benign skin tumours, which could accelerate diagnostic and therapeutic procedures in dermatology. The recently available integration of FM, RM, OM and DS allows a better diagnostic assessment and enables an immediate comparison with histology. Further studies are necessary to better investigate the accuracy of ex vivo CLSM in different skin pathologies to extend its field of application.

CONFLICT OF INTEREST
The Vivascope 2500M-G4 device was provided by Mavig GmbH for the time of the study from January to May 2019. All authors declare no financial or personal relationship connected to this project that could be viewed as potential conflict of interest.

DATA AVAILABILITY STATEMENT
The data that support the findings of this study are available on request from the corresponding author. The data are not publicly available due to privacy or ethical restrictions.

ORCID
Cristel Ruini https://orcid.org/0000-0002-9860-1095
Sebastian Krammer https://orcid.org/0000-0001-7968-9821

REFERENCES

[1] U. Leiter, T. Eigentler, C. Garbe, *Adv. Exp. Med. Biol.* **2014**, *810*, 120.

[2] C. Garbe, K. Peris, E. Soura, A. M. Forsea, A. Hauschild, M. Arenbergerova, M. Bylaite, V. Marmol, V. Bataille, M. Samimi, S. Gandini, P. Saiag, T. K. Eigentler, A. Lallas, I. Zalaudek, C. Lebbe, J. J. Grob, C. Hoeller, C. Robert, B. Dréno, P. Arenberger, L. Kandolf-Sekulovic, R. Kaufmann, J. Malvehy, S. Puig, U. Leiter, S. Ribero, E. Papadavid, P. Quaglino, M. Bagot, S. M. John, M. A. Richard, M. Trakatelli, C. Salavastru, L. Borradori, B. Marinovic, A. Enk, C. Pincelli, D. Ioannides, C. Paul, A. J. Stratigos, *J. Eur. Acad. Dermatol. Venereol.* **2020**, *34*(10), 2183.

[3] E. Cinotti, J. L. Perrot, B. Labeille, F. Cambazard, P. Rubegni, *Dermatol. Pract. Concept.* **2018**, *8*(2), 109.

[4] E. Cinotti, V. Belgrano, B. Labeille, D. Grivet, C. Douchet, C. Chauleur, F. Cambazard, A. Thomas, V. Prade, L. Tognetti, A. Cartocci, P. Rubegni, J. L. Perrot, *J. Biophotonics* **2020**, *13*(11), e202000179.

[5] A. Lamberti, E. Cinotti, C. Habougit, B. Labeille, P. Rubegni, J. L. Perrot, *Skin Res. Technol.* **2019**, *25*(4), 589.

[6] D. Hartmann, C. Ruini, L. Mathemeier, M. R. Bachmann, A. Dietrich, T. Ruzicka, T. von Braunmühl, *J. Biophotonics* **2017**, *10*(1), 128.

[7] A. Villarreal-Martinez, A. Bennàssar, S. Gonzalez, J. Malvehy, S. Puig, *Br. J. Dermatol.* **2018**, *178*(5), 1215.

[8] E. Cinotti, J. L. Perrot, B. Labeille, N. Campolmi, G. Thuret, N. Naigeon, T. Bourlet, S. Pillet, F. Cambazard, *Clin. Exp. Dermatol.* **2015**, *40*(4), 421.

[9] S. Krammer, C. Krammer, G. Vladimirova, S. Salzer, C. Ruini, E. Sattler, L. E. French, D. Hartmann, *Front. Med. (Lausanne).* **2020**, *7*, 586648.

[10] L. Bertoni, P. Azzoni, C. Reggiani, A. Pisciotta, G. Carnevale, J. Chester, S. Kaleci, L. Reggiani Bonetti, A. M. Cesinaro, C. Longo, G. Pellacani, *Exp. Dermatol.* **2018**, *27*(10), 1152.

[11] D. Hartmann, C. Ruini, L. Mathemeier, A. Dietrich, T. Ruzicka, T. von Braunmühl, *J. Biophotonics* **2016**, *9*(4), 376.

[12] D. Hartmann, S. Krammer, S. Vural, M. R. Bachmann, C. Ruini, M. Sárdy, T. Ruzicka, C. Berking, T. von Braunmühl, *J. Biophotonics* **2018**, *11*(3), e201700211.

[13] I. S. Bağcı, R. Aoki, S. Krammer, T. Ruzicka, M. Sárdy, D. Hartmann, *J. Biophotonics* **2019**, *12*(9), e201800425.

[14] I. S. Bağcı, R. Aoki, S. Krammer, T. Ruzicka, M. Sárdy, L. E. French, D. Hartmann, *J. Eur. Acad. Dermatol. Venereol.* **2019**, *33*(11), 2123.

[15] S. Krammer, C. Krammer, S. Salzer, I. S. Bağcı, L. E. French, D. Hartmann, *Front. Med. (Lausanne).* **2019**, *6*, 262.

[16] I. S. Bağcı, R. Aoki, G. Vladimirova, M. Sárdy, T. Ruzicka, L. E. French, D. Hartmann, *J. Biophotonics* **2021**, *14*, e202000509.

[17] I. S. Bağcı, R. Aoki, G. Vladimirova, E. Ergün, T. Ruzicka, M. Sárdy, L. E. French, D. Hartmann, *Exp. Dermatol.* **2021**, *30*(5), 684.

[18] I. S. Bağcı, R. Aoki, S. Krammer, G. Vladimirova, T. Ruzicka, M. Sárdy, L. E. French, D. Hartmann, *J. Biophotonics* **2020**, *13*(12), e202000328.

[19] C. Longo, R. Pampena, C. Bombonato, S. Gardini, S. Piana, M. Mirra, M. Raucci, A. Kyrgidis, G. Pellacani, M. Ragazzi, *Br. J. Dermatol.* **2019**, *180*(6), 1473.

[20] A. Bennàssar, A. Vilata, S. Puig, J. Malvehy, *Br. J. Dermatol.* **2014**, *170*(2), 360.

[21] C. Longo, M. Ragazzi, M. Rajadhyaksha, K. Nehal, A. Bennassar, G. Pellacani, J. Malvehy Guilera, *Dermatol. Clin.* **2016**, *34*(4), 497.

[22] D. Hartmann, S. Krammer, M. R. Bachmann, L. Mathemeier, T. Ruzicka, I. S. Bagci, T. von Braunmühl, *J. Biophotonics* **2018**, *11*(4), e201700318.

[23] D. Hartmann, S. Krammer, M. R. Bachmann, L. Mathemeier, T. Ruzicka, T. von Braunmühl, *J. Biophotonics* **2018**, *11*(7), e201800062.

[24] D. Hartmann, S. Krammer, C. Ruini, T. Ruzicka, T. von Braunmühl, *Lasers Med. Sci.* **2016**, *31*(5), 921.

[25] M. Grupp, M. Illes, J. Mentzel, J. C. Simon, U. Paasch, S. Grunewald, *J. Dtsch. Dermatol. Ges.* **2021**, *19*(5), 685.

[26] M. Schüürmann, M. M. Stecher, U. Paasch, J. C. Simon, S. Grunewald, *J. Eur. Acad. Dermatol. Venereol.* **2020**, *34*(7), 1496.

[27] J. Pérez-Anker, S. Puig, J. Malvehy, *J. Am. Acad. Dermatol.* **2020**, *82*(5), e157.

[28] A. Bennàssar, C. Carrera, S. Puig, A. Vilalta, J. Malvehy, *JAMA Dermatol.* **2013**, *149*(7), 839.

[29] DescTools: Tools for Descriptive Statistics 2020 [R package version 0.99.38], https://cran.r-project.org/package=DescTools (accessed: September 2021).

[30] X. Robin, N. Turck, A. Hainard, N. Tiberti, F. Lisacek, J. Sanchez, M. Müller, *BMC Bioinform.* **2011**, *12*, 77.

[31] H. Wickham, *ggplot2: Elegant Graphics for Data Analysis*, Springer-Verlag New York, Boston, MA. ISBN 978-3-319-24277-4, **2016**. https://ggplot2.tidyverse.org (accessed: September 2021).

[32] J. Pérez-Anker, S. Ribero, O. Yélamos, A. García-Herrera, L. Alos, B. Alejo, M. Combalia, D. Moreno-Ramírez, J. Malvehy, S. Puig, *Br. J. Dermatol.* **2020**, *182*(2), 468.

[33] C. Reggiani, G. Pellacani, L. Reggiani Bonetti, G. Zanelli, P. Azzoni, J. Chester, S. Kaleci, B. Ferrari, P. Bellini, C. Longo, L. Bertoni, C. Magnoni, *J. Eur. Acad. Dermatol. Venereol.* **2021**, *35*(1), e92.